Geophysical Research Letters

RESEARCH LETTER
10.1029/2022GL100460

Key Points:

- Float profiles show warm (up to −0.16°C) modified Circumpolar Deep Water at depth in a trough extending below the Denman Ice Tongue
- A bottom-intensified current on the eastern side of the deep trough transports 138 ± 65 mSv of water warmer than −1°C into the cavity
- Ocean heat transport into the cavity is sufficient to drive high basal melt (70.8 ± 31.5 Gt y^{-1}), consistent with glaciological observations

Supporting Information:

Supporting Information may be found in the online version of this article.

Correspondence to:

E. M. van Wijk,
Esmee.vanWijk@csiro.au

Citation:

van Wijk, E. M., Rintoul, S. R., Wallace, L. O., Ribeiro, N., & Herraiz-Borreguero, L. (2022). Vulnerability of Denman Glacier to ocean heat flux revealed by profiling float observations. *Geophysical Research Letters*, *49*, e2022GL100460. https://doi.org/10.1029/2022GL100460

Received 19 JUL 2022
Accepted 2 SEP 2022

Author Contributions:

Conceptualization: Esmee M. van Wijk, Stephen R. Rintoul
Data curation: Esmee M. van Wijk
Formal analysis: Esmee M. van Wijk, Stephen R. Rintoul
Funding acquisition: Stephen R. Rintoul
Investigation: Esmee M. van Wijk, Stephen R. Rintoul, Luke O. Wallace, Natalia Ribeiro, Laura Herraiz-Borreguero
Methodology: Esmee M. van Wijk, Stephen R. Rintoul
Resources: Stephen R. Rintoul
Validation: Esmee M. van Wijk, Stephen R. Rintoul, Luke O. Wallace, Natalia Ribeiro
Visualization: Esmee M. van Wijk, Stephen R. Rintoul, Luke O. Wallace, Natalia Ribeiro, Laura Herraiz-Borreguero

Vulnerability of Denman Glacier to Ocean Heat Flux Revealed by Profiling Float Observations

Esmee M. van Wijk[1,2], Stephen R. Rintoul[1,2,3], Luke O. Wallace[4], Natalia Ribeiro[5], and Laura Herraiz-Borreguero[1,3]

[1]CSIRO Oceans and Atmosphere, Hobart, TAS, Australia, [2]Australian Antarctic Program Partnership, University of Tasmania, Hobart, TAS, Australia, [3]Centre for Southern Hemisphere Oceans Research, Hobart, TAS, Australia, [4]School of Geography, Planning and Spatial Sciences, University of Tasmania, Hobart, TAS, Australia, [5]Institute for Marine and Antarctic Studies, University of Tasmania, Hobart, TAS, Australia

Abstract Denman Glacier, which drains a marine-based sector of the East Antarctic Ice Sheet with an ice volume equivalent to 1.5 m of global sea level rise, has accelerated and undergone grounding line retreat in recent decades. A deep trough and retrograde bed slope inward of the grounding line leave this glacier prone to marine ice sheet instability. The ocean heat flux to the ice shelf cavity is a critical factor determining the susceptibility of the glacier to unstable retreat. Profiling float observations show modified Circumpolar Deep Water as warm as −0.16°C reaches a deep trough extending beneath the Denman Ice Tongue. The ocean heat transport (0.77 ± 0.35 TW) is sufficient to drive high rates of basal melt (70.8 ± 31.5 Gt y^{-1}), consistent with rates inferred from glaciological observations. These results suggest the Denman Glacier is potentially at risk of unstable retreat triggered by transport of warm water to the ice shelf cavity.

Plain Language Summary The Denman Glacier is a vast river of ice that drains the East Antarctic Ice Sheet. The Denman holds a volume of ice equivalent to 1.5 m of global sea level rise, so changes in the glacier could have a large impact on future sea level rise. The vulnerability of the Denman Glacier to melting by warm ocean waters has been difficult to assess because very few oceanographic observations have been collected in the region. We use new profiling float measurements to show warm water reaches a deep trough that extends inland beneath the glacier, exposing the base of the ice to ocean-driven melting. We estimate that the amount of warm water entering the cavity is sufficient to melt 70.8 billion tons of ice each year. These observations suggest that the Denman Glacier is potentially at risk from unstable retreat driven by warm water flowing into the cavity and melting the ice from below.

1. Introduction

The Denman Glacier is a major drainage of the East Antarctic Ice Sheet, containing an ice volume equivalent to 1.5 m of global sea level rise (Rignot et al., 2019). The deep trough beneath the glacier (extending more than 3,500 m below sea level) and the retrograde bed slope make the Denman Glacier potentially susceptible to marine ice sheet instability (Miles et al., 2021; Morlighem et al., 2020). Recent studies have documented grounding line retreat (Brancato et al., 2020) and acceleration of the Denman Glacier in recent decades (Miles et al., 2021; Rignot et al., 2019).

Our understanding of the drivers of grounding line retreat of the Denman Glacier have been hampered by sparse bathymetric and oceanographic observations near the Denman Ice Tongue (DIT) and adjacent continental shelf. Glaciological estimates of high basal melt rates (e.g., >45 ± 4 m a^{-1}) suggest that warm water likely reaches the grounding line (Brancato et al., 2020; Liang et al., 2021). However this inference has been difficult to confirm through direct observations, as persistent sea ice cover makes this region difficult to access and observe by ship. Oceanographic observations in the region have been limited to five profiles, one near the ice front, collected by an instrumented elephant seal in 2011 (Brancato et al., 2020). Two of the profiles showed warm water at depth in a deep trough on the shelf (Brancato et al., 2020), providing the first direct evidence that warm water reached the Denman continental shelf and the deep trough that leads beneath the Denman Glacier. However, the single seal profile near the ice front was insufficient to calculate how much warm water entered the ice shelf cavity.

Here we report on new oceanographic measurements collected by a profiling float on the continental shelf near the DIT, including a transect along the ice front that allows us to estimate the transport into the ice shelf cavity.

Writing – original draft: Esmee M. van Wijk, Stephen R. Rintoul
Writing – review & editing: Esmee M. van Wijk, Stephen R. Rintoul, Luke O. Wallace, Natalia Ribeiro, Laura Herraiz-Borreguero

The float measurements of temperature and salinity show that warm modified Circumpolar Deep Water (mCDW) fills the bottom of a deep trough leading beneath the glacier. We show that warm water enters the cavity along the eastern flank of the trough, carrying sufficient heat to drive high rates of basal melt.

2. Methods

2.1. Profiling Float Observations

A profiling float (WMOID: 7900904) collected observations near the DIT from 9 December 2020 (Figure 1a, red star). The float remained on the continental shelf off the Denman Glacier for 4 months, collecting 23 profiles at approximately 5-day intervals. Between profiles, the float drifted at 285 dbar, completing a clockwise loop and passing along the front of the DIT. The float last reported on 26 March 2021 before disappearing under winter sea ice. The float utilized an ice-avoidance algorithm similar to Klatt et al. (2007) and was programmed to profile to the seafloor on the shelf. The 2-dbar conductivity-temperature-depth (CTD) data were delayed-mode quality controlled and are accurate to ±0.01 for salinity, ±0.002°C for temperature and ±2.4 dbar for pressure (Wong et al., 2021). The float surfaced and obtained a Global Positioning System (GPS) fix for 12 of the 23 profiles measured on the shelf (Figure 1b). Profiles beneath sea ice with missing GPS locations were linearly interpolated between known positions. Given large discrepancies between seafloor depths measured by the float and the bathymetry (Figures 1c and 1d), it was not possible to use the technique described in Wallace et al. (2020) to determine the location of profiles without a GPS fix. The uncertainty in the linearly interpolated positions is assessed in Supporting Information S1 (Figure S1, Text S1).

2.2. Meltwater Fraction

We use the method of Jenkins (1999) to estimate the basal meltwater fraction from potential temperature and salinity (no oxygen data are available from the float). The method assumes that the ambient water is a mixture of two water masses (in this case, Winter Water (WW) and mCDW). Meltwater input results in a deviation from the mixing line defined by the two ambient end-member water masses. We use the warmest and saltiest mCDW (−0.2°C, 34.61) and coldest, saltiest WW (−1.8°C, 34.419) as end-members to define the mCDW-WW mixing line. The temperature of pure meltwater (−92°C) is obtained by extrapolating the mCDW-meltwater mixing line to zero salinity (Gade, 1979).

2.3. mCDW Transport

The transport of mCDW into the cavity was calculated using the geostrophic relationship (Texts S2–S4 in Supporting Information S1). Following earlier studies of ocean exchange with ice shelf cavities (e.g., Dutrieux et al., 2014; Jacobs et al., 2011; Jenkins & Jacobs, 2008), we choose a reference level based on the assumption that water with lower concentrations of meltwater are likely to be entering the cavity, while water with higher concentrations of meltwater are likely to be exiting the cavity. In this case, we use the 2 per mil contour of meltwater fraction as the reference level. The 2 per mil contour roughly coincides with the bottom of the WW layer. The sensitivity to this choice is assessed in Text S3 in Supporting Information S1. Note that the geostrophic transport between two profiles with known positions is not sensitive to errors in the position of intermediate profiles.

The geostrophic velocity is not defined below the deepest common depth of each profile pair. To estimate transport in the "bottom triangle" below the deepest common depth, we assumed constant velocity below this depth. This assumption is likely conservative, as the vertical shear just above the deepest common depth suggests an increase of velocity toward the bottom. Direct current measurements in a similar deep trough adjacent to the Totten Ice Shelf found current speed increased to a maximum at the seafloor (Rintoul et al., 2016). The sensitivity to this choice is discussed below and in Table S1, Text S3 of Supporting Information S1.

2.4. Volume Exchange With the Cavity Estimated From Satellite-Derived Basal Melt

The observed temperatures of the inflow and outflow layers can be used to provide an estimate of the volume exchange with the cavity that is independent of the velocity estimates used in the transport calculation. Following Wilson and Straneo (2015), we assume a two-layer estuarine circulation in which warm water enters the cavity,

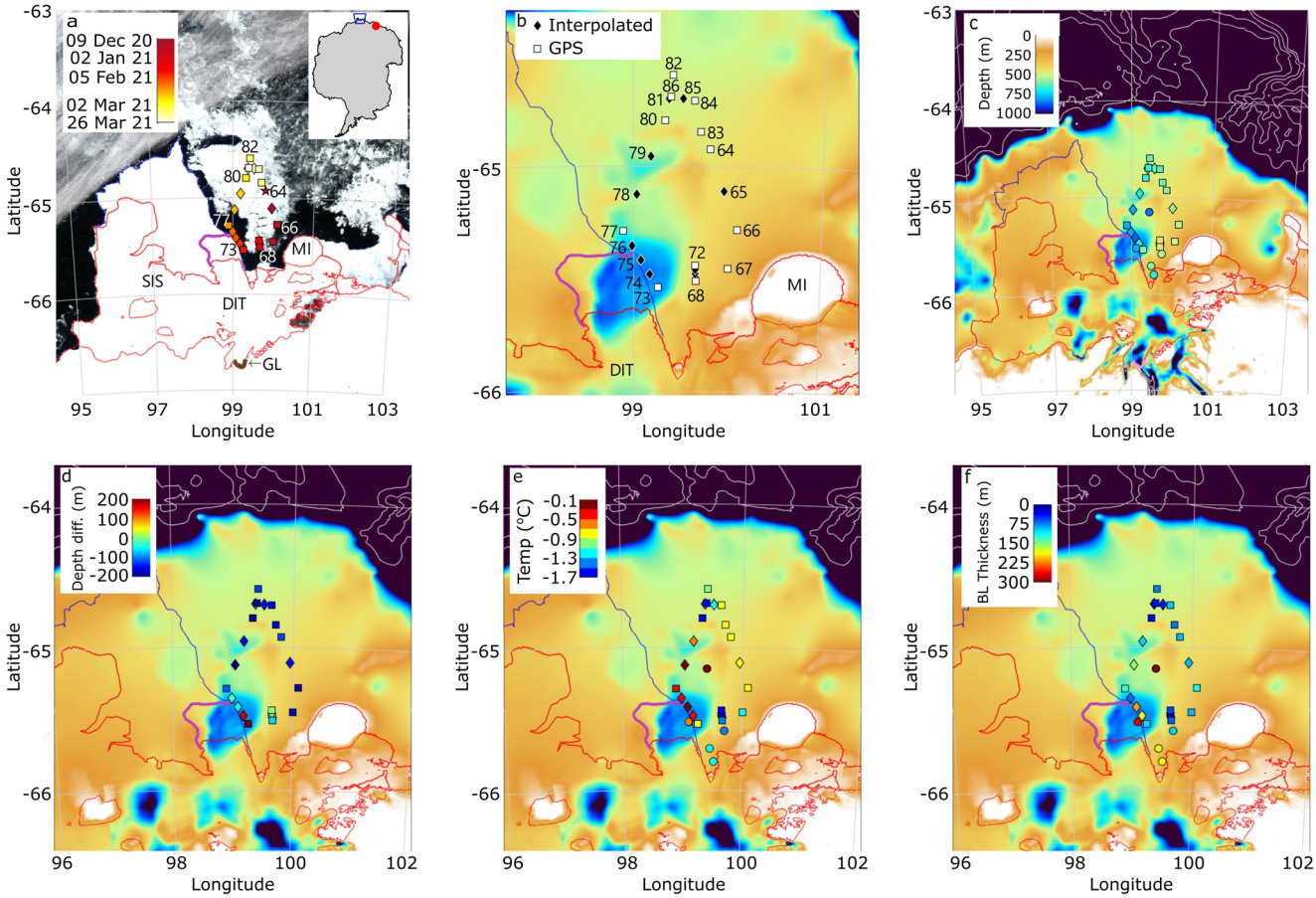

Figure 1. (a) MODIS image (23 January 2021) of Denman Ice Tongue (DIT), Shackleton Ice Shelf (SIS) and Mill Island (MI) and profile locations. Inset (at top right) indicates location of Denman region (blue square) and Totten Glacier (red dot). Color bar indicates profile date; star indicates first profile on the shelf. Squares (star) are float profiles with Global Positioning System (GPS) position; diamonds are linearly-interpolated under-ice positions. The bold line segment labeled GL marks the grounding line of the Denman Glacier. (b) Profile locations (c) Water depth (m) from grounded float profiles (circles are seal profiles from 2011, Brancato et al., 2020). (d) Difference between bathymetry and float depth (m), negative values indicate float is deeper. (e) Modified Circumpolar Deep Water (mCDW) temperature (°C) at maximum profile depth. (f) mCDW bottom layer (BL) thickness. Solid red lines are the grounding line (southern) and ice shelf edge (northern) from Morlighem (2020). Position of the DIT (purple line) and fast ice edge (blue line) digitised from Sentinel_2 image 16 February 2021. Bathymetry in panels (b–f) is from BedMachine_v2 (Morlighem, 2020). Color bar for bathymetry in panels (b, d–f) as for panel (c). White depth contours are at 1,500, 2,000, 2,500, and 3,000 m.

drives basal melt, and a mixture of meltwater and mCDW leaves the cavity. Given a known satellite-derived basal melt rate, and the temperature of the inflow and outflow, the heat budget can be used to estimate the exchange rate $M = L_f M_{\text{melt}}/C_w(T_{\text{in}}–T_{\text{out}})$, where M is the exchange rate, L_f is the latent heat of fusion (334 kJ kg^{-1}), C_w is the specific heat capacity of seawater (3.985 kJ kg^{-1} K^{-1}), M_{melt} is the flux of meltwater, and T_{in} and T_{out} are the potential temperatures of the inflow and outflow.

3. Results

3.1. Water Properties on the Continental Shelf

Modified CDW is found near the seafloor on all float profiles on the continental shelf (Figure 1e). Modified CDW bottom layer thickness, defined as the layer with potential density anomaly referenced to the surface (σ_θ) > 27.7 kg m^{-3} (Silvano et al., 2017), ranged from 17 to 215 m, with a mean ± standard deviation of 85 ± 51 m (Figure 1f). The warmest bottom layers are also the thickest (101–215 m, Figures 1e and 1f). Airborne geophysical measurements identified a deep trough adjacent to the DIT (Brancato et al., 2020). The warmest in situ temperatures measured by the float (−0.36 to −0.16°C) were in this deep trough, at depths of 578–875 m (Figures 1c and 1e). For 11 of 12 profiles with known positions, the depths measured by the float are significantly deeper (mean ± standard deviation of 147 ± 38 m) than the bathymetry (Figures 1c and 1d). Seafloor depths

measured by the float (and seals; Figure S3, Text S5 in Supporting Information S1) show that the deep trough may be considerably deeper and extend further north than inferred from the gravity data.

3.2. Vertical Sections of Water Mass Properties

Vertical sections of potential temperature (θ) and salinity reveal three layers: a relatively fresh and light surface mixed layer; an intermediate layer with temperatures near the surface freezing point and salinity gradually increasing with depth; and a warm, saline layer of mCDW near the seafloor (Figure 2). The cold mid-depth waters are separated from the warmer mCDW by a sharp thermocline. The depth of the thermocline varies from profile to profile and is related to seafloor depth, with deeper thermoclines found in deeper water.

The thickest and warmest mCDW layers ($\theta > -0.6$°C) are found in the deep trough near the DIT (profiles 73–78, Figures 2a–2d). The mCDW layer is cooler ($\theta < -0.7$°C) and thinner along the eastern section, where the seafloor depths are shallower (Figures 2e–2h). Note that the sharp gradients observed in the upper ocean between profiles 64 and 83 are likely influenced by temporal changes in ocean structure over the 3-month gap in time between when the profiles were sampled.

While the temperature of the intermediate layer is relatively uniform, salinity (and therefore density) increases with depth through this layer (Figures 2a–2f). Consistent with previous literature, we refer to this layer as WW, but note that the layer is stratified in salinity and is not well-mixed as would be expected for a remnant deep mixed layer. The gradual decrease in salinity with height through the WW layer can be explained by inflow of glacial melt water. The melt water fraction (white contours, Figures 2c, 2d, 2g, and 2h) increases upward through the WW layer, reaching values of about 5 per mil near the top of the WW thermostad (higher values in the surface layer likely reflect air-sea interaction rather than meltwater input (Jenkins, 1999)). The layer enriched in meltwater (e.g., with meltwater fraction > 3 per mil) is thickest immediately to the north of the DIT (profiles 77–79, Figure 2d), consistent with outflow from the cavity on the western side of the deep trough. The layer with > 3 per mil meltwater fraction is thinner on the eastern section (Figures 2g and 2h), consistent with recirculation of some meltwater to the east.

3.3. Potential Temperature—Salinity Properties

The θ-S relationship for profiles near the DIT is shown by the blue curves in Figure 3. The linear portion corresponds with the sharp thermocline/halocline between warm, salty mCDW and the overlying cold WW. The curved portion extending from salinities of 34.3–34.4 at potential temperatures of about −1.8°C coincides with the WW layer. The most saline WW (lower black square in Figure 3) is used as the end-member for the meltwater fraction calculation (after Jenkins, 1999). The meltwater fraction increases (and salinity decreases) with height above the mCDW layer (Figures 2c, 2d, 2g, and 2h), indicating larger input of glacial meltwater at shallower levels.

The shape of the θ-S curve near the Denman ice front is reminiscent of the θ-S curve observed in front of the Totten Glacier (red curves, Figure 3). At both ice shelves, the warm mCDW layer that enters the ice shelf cavity is relatively thin and does not occupy the entire ice shelf cavity (Figure 2 and Figure 2 of Rintoul et al. (2016)). Meltwater ascends and mixes with WW before it exits the cavity. Water found at intermediate depth on the continental shelf is therefore a three-way mixture of mCDW, WW and glacial meltwater (a two-way mixture of mCDW and meltwater would fall on the dashed gray mixing line (Gade line), which is not observed). Water on the continental shelf at Totten is fresher than at Denman, likely reflecting larger combined meltwater inputs from the Totten and Moscow University Ice Shelves (Rignot et al., 2019).

3.4. Velocity and Transport

Near the DIT (profiles 73–76), the mCDW layer is banked up on the eastern side of the deep trough: while the warmest water is seen at the deepest profile (profile 75, in situ $T = -0.16$°C, 875 dbar), water warmer than $\theta = -0.4$°C is found as shallow as 600 dbar over the south-eastern flank of the trough (profile 74, Figure 2a). The tilt of density layers results in geostrophic shear on the south-eastern flank of the trough. Relative to the 2 per mil meltwater fraction contour (see Sections 2.2–2.3), the geostrophic inflow to the cavity reaches a maximum of 11 cm s^{-1} between profiles 74 and 75 (Figure S2 and Text S2 in Supporting Information S1). The net transport of

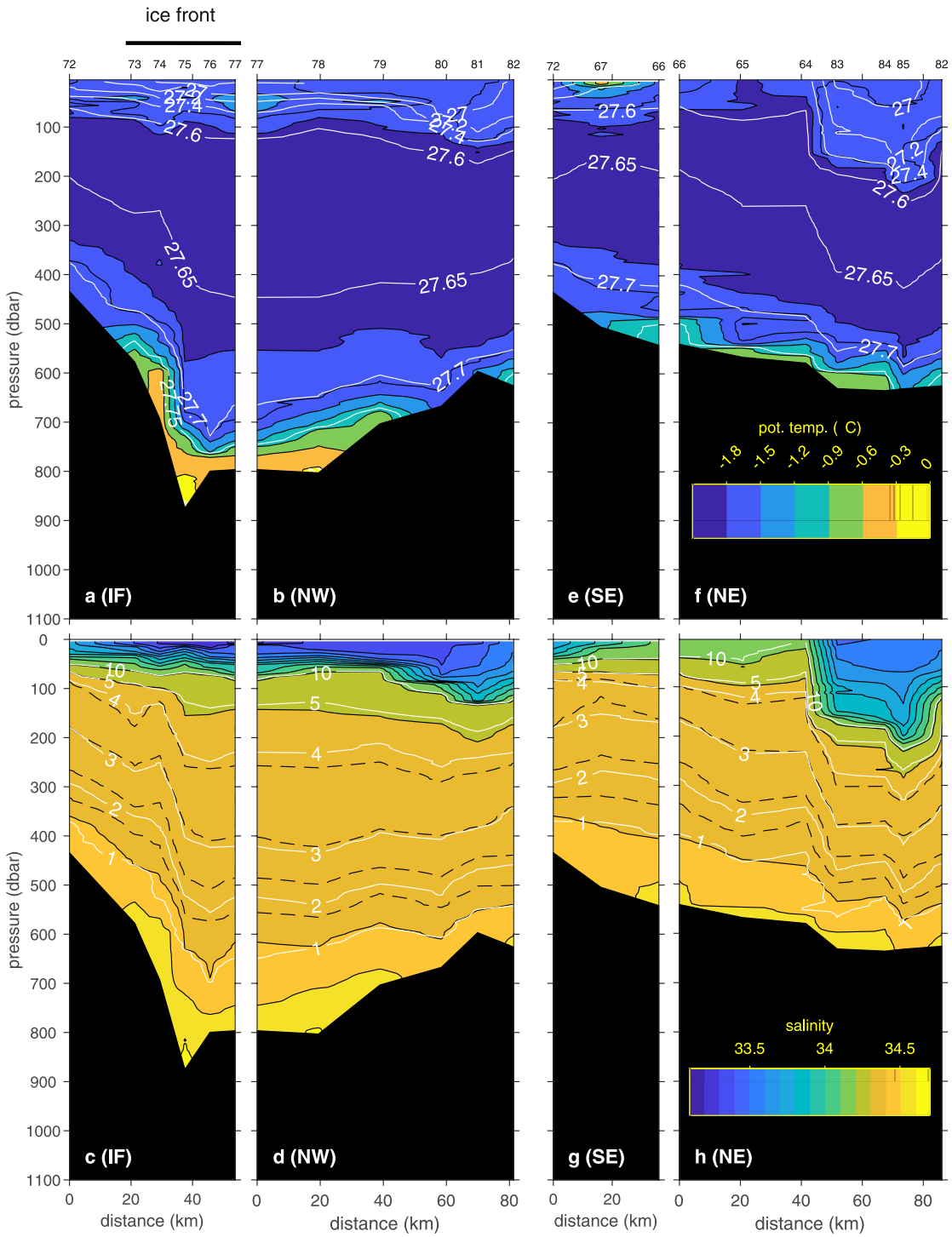

Figure 2. Potential temperature (°C; top) and practical salinity (psu; bottom) on the western (left) and eastern (right) sides of the float trajectory shown in Figure 1. Potential density (σ_θ, kg m^{-3}) is overlaid on temperature (white contours, top row); meltwater fraction is overlaid on salinity (white contours, bottom row). The float trajectory is divided into four sections, IF = Ice Front, NW = northwest leg, SE = southeast leg, NE = northeast leg; the northern end of each section is to the right. Contour intervals are 0.3°C, 0.05 kg m^{-3}, 0.1, and 0.02 (dashed contours) for salinity, and 1 per mil from 0 to 5 per mil plus the 10 per mil contour for meltwater fraction. The black bar labeled "ice front" indicates float profiles directly adjacent to the DIT. Profile number is labeled on the top axis.

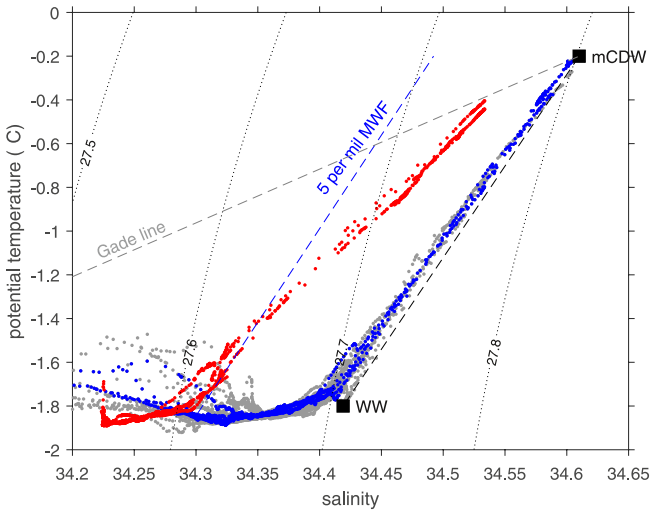

Figure 3. Potential temperature-salinity properties near the Denman (blue, profiles 73–77) and Totten (red, profiles 34–36; Rintoul et al. (2016)) ice shelves. Surface waters fresher than 34.2 not shown. Black squares indicate modified Circumpolar Deep Water (mCDW) (−0.2°C, 34.61) and WW (−1.8°C, 34.419) properties used as end-members for the meltwater fraction calculation. Dashed blue line is the 5 per mil meltwater fraction contour for the Denman profiles. Dashed gray line is the mixing line between mCDW and pure glacial meltwater (the Gade line, Gade (1979)). Gray contours indicate potential density (0.1 kg m^{-3} spacing). θ–S properties for profiles on the Denman continental shelf, distant from the ice front, are shown as gray dots.

water warmer than $\theta = -1$°C entering the cavity between profiles 73 and 77 is 138 ± 65 × 10^3 m^3 s^{-1} (mSv), where the error bar represents the range of transports obtained when varying the reference level and treatment of transport in the bottom triangles (Table S1 and Text S3 in Supporting Information S1). The net transport between profiles 73 and 77 should represent the total deep inflow of warm water to the cavity, as this section nearly spans the only known deep access to the ice shelf cavity (Figure 1b). The baroclinic transport is likely to dominate the heat transport to the cavity, as barotropic flows are blocked by the step change in water column thickness at the ice front (Wåhlin et al., 2020).

Assuming the net inflow of warm water across the ice front section (profiles 73 to 77) is balanced by outflow of water with a potential temperature of −1.85°C (the mean temperature of the WW layer), the ocean heat transport into the cavity is 0.77 ± 0.35 TW (Text S4 in Supporting Information S1). This ocean heat flux is sufficient to produce 70.8 ± 31.5 Gt y^{-1} (equivalent to a volume transport of 2.3 ± 1.0 mSv) of basal melt.

The transport estimated from ocean observations at the ice front can be compared to the exchange rate implied by basal melt rates inferred from satellite data, assuming that the basal melt is driven by ocean heat flux. Setting T_{in} to the transport-weighted temperature of the inflowing mCDW (−0.48°C) and T_{out} to the mean temperature of the WW layer at the ice front (−1.85°C), the basal melt of 54.6 ± 7.2 Gt y^{-1} inferred from Cryosat-2 data by Liang et al. (2021) implies an exchange rate of 104 ± 14 mSv. Liang et al. (2021) note that their estimate may be low because of gaps in coverage near the rapidly-melting grounding line. The basal melt rate estimates of Rignot et al. (2013) (72.6 ± 15 Gt y^{-1}) and Depoorter et al. (2013) (76 ± 23 Gt y^{-1}) imply exchange rates of 139 ± 29 mSv and 145 ± 44 mSv, respectively. The model-based estimate of Bernales et al. (2017) of 88.7 Gt y^{-1} requires an exchange rate of 169 mSv. The exchange rates inferred from satellite- and model-based estimates of basal melt are therefore consistent with the geostrophic transport estimated from the float data (138 ± 65 mSv).

4. Discussion and Conclusions

We use profiles of temperature and salinity collected by a profiling float near the Denman Glacier, including the first transect along the front of the ice tongue, to assess the vulnerability of the Denman Glacier to ocean-driven melt. Warm mCDW is widespread on the continental shelf, occupying a layer on the seafloor that ranges from 17 to 215 m in thickness. The thickest and warmest mCDW layers ($\theta > -0.6$°C, maximum in situ temperature = −0.16°C) are observed in a deep trough adjacent to the DIT.

The observation of warm water in the deep trough adjacent to the DIT is reminiscent of the Totten Ice Shelf, where strong inflow of warm water was found to carry sufficient heat transport to explain high rates of basal melt inferred from satellite data (Rintoul et al., 2016). The similarity between the two systems extends further. The inflow of water warmer than −1.0°C is smaller at Denman (138 ± 65 mSv) than at Totten (220 ± 70 mSv), but the transport-weighted temperature is higher (−0.48°C at Denman vs. −0.81°C at Totten), resulting in ocean heat transports and meltwater production rates that agree within error bars (ocean heat flux sufficient to form 2.3 ± 1.0 mSv of meltwater at Denman, compared to 2.8 ± 0.9 mSv at Totten). The float measurements confirm that the Denman Glacier, like the Totten Glacier, is exposed to ocean heat transport sufficient to drive high rates of basal melt (70.8 ± 31.5 Gt y^{-1}), as inferred from independent glaciological observations.

The deep trough adjacent to the DIT is part of a sub-glacial channel that extends inland and reaches depths >3,500 m below sea level (Morlighem et al., 2020). However, the channel is not continuously deep along its length. Three ridges cross the channel with depths of about 500 m (Brancato et al., 2020). The warmest water found in the deep trough adjacent to the ice tongue may therefore be blocked from accessing the grounding line. However, the steep tilt of the isopycnals on the southeastern flank of the deep trough facilitates access of warm

water to the cavity, both by elevating warm water to shallower levels where it may be able to cross the ridges, and through the geostrophic inflow associated with sloping isopycnals. In addition, we note that measurements of seafloor depth from the float and seals are generally deeper (by 147 and 65 m, respectively) than bathymetry derived from gravity measurements, which have an uncertainty of 150–200 m in the vertical (Brancato et al., 2020) and may not resolve narrow channels that cross the ridges (if present). Therefore, it is possible that warm water has access to the grounding line. Indeed, the high basal melt rates inferred from glaciological observations imply that warm water reaches the grounding line (Brancato et al., 2020; Liang et al., 2021).

Estimates of the melt rate near the grounding line of the Denman Glacier are higher than for other glaciers in East Antarctica and rival melt rates of rapidly thinning glaciers in West Antarctica. Melt rates at the grounding line of 45 ± 4 m a^{-1} between 2011 and 2014 (Brancato et al., 2020) and 50 m a^{-1} between 2010 and 2018 (Liang et al., 2021) imply strong ocean thermal forcing. If the warmest water we observed on the shelf can reach the grounding line, the maximum thermal forcing is 3.1°C, the difference between the warmest in situ temperature at the DIT front (−0.16°C) and the freezing temperature at 1,800 dbar (−3.26°C). Given that ridges crossing the deep channel beneath the Denman may limit the inflow of the warmest water, the ocean thermal forcing appears to be too low to drive the high melting rates inferred near the grounding line, if the simple relationship between ocean temperature and melt rate derived by Rignot and Jacobs (2002) applies to the Denman. Melting rates in the grounding zone (the region immediately seaward of the grounding line where tides drive intermittent grounding and ungrounding of the ice shelf) are estimated to be 10–20 m a^{-1} (Brancato et al., 2020), a rate that could be supported by the observed ocean thermal forcing. Very high melt rates near the grounding line of the Pine Island Glacier have recently been attributed to subglacial freshwater discharge, but the influence on melt rates was found to be limited to the immediate vicinity of the grounding line (Nakayama et al., 2021). A similar situation may hold for the Denman, with subglacial freshwater discharge contributing to high melt rates at the grounding line and ocean thermal forcing driving lower, but more widespread, basal melt. The melt rate will be determined by the ocean heat flux that reaches the base of the ice shelf, which is affected by the bathymetry, circulation, tides, vertical mixing, plume dynamics, and ice shelf draft and shape (Jenkins, 2011; MacAyeal, 1984; Makinson, 2002; Rignot & Jacobs, 2002). Further work and more observations are required to understand how these factors interact to regulate melt of the Denman ice shelf.

The pathway followed by warm mCDW from the outer shelf to the DIT is not clear. The float observations suggest there is inflow from the east of relatively cool mCDW ($\theta < -0.7$°C). The warmer mCDW ($\theta > -0.6$°C) observed on the western and southern legs of the float trajectory implies a deep channel may exist in the poorly-sampled area to the north of the survey region. Comparison of water depths measured by the float and seals suggests that present bathymetry estimates are too shallow over the continental shelf (Figure S3, Text S5 in Supporting Information S1). Seal profiles in the vicinity of three outer shelf troughs show some warmer water near the seafloor and deeper depths than in the bathymetry products. Warmer water in the troughs is consistent with measurements of temperature offshore (Yamazaki et al., 2020), which show the temperature maximum waters over the slope are warmer and shallower near two outer-shelf troughs directly north of the DIT. Moreover, dynamic height minima associated with isopycnal shoaling are seen just offshore of these two troughs near 98–102°E (Yamazaki et al., 2020). This localized isopycnal shoaling may facilitate access of warm CDW to the troughs that provide access to the shelf. While these results are suggestive, measurements of seafloor depth and temperature are still too sparse to identify inflow pathways with confidence.

Glaciological observations have documented a long-term acceleration of the Denman Glacier. For example, Rignot et al. (2019) estimated a 16% increase in flow speed of the glacier since the 1970's, while Miles et al. (2021) found accelerations of 17 ± 4% (grounded portion) and 36 ± 5% (floating portion) between 1972 and 2017. For the recent short period between 2017 and 2021, no acceleration was found (Thompson et al., 2021). The grounding line of the Denman Glacier retreated by 5.4 ± 0.3 km between 1996 and 2017–2018 (Brancato et al., 2020). The changes in glacial flow may reflect an increase in ocean heat transport to the base of the glacier and/or ice dynamics (i.e., ice tongue thinning, changes in ice tongue structure following calving, or release from pinning points) (Miles et al., 2021; Rignot et al., 2019). While changes in ocean heat transport cannot be assessed with available observations, recent studies have documented warming of waters off East Antarctica that may have increased ocean heat transport to the continental shelf (e.g., Herraiz-Borreguero & Naveira Garabato, 2022; Yamazaki et al., 2021).

Several caveats must be kept in mind when interpreting our results. The float profiles provide the first detailed oceanographic information near the DIT, but the float only provides a snapshot from a single season with limited spatial coverage. Further observations from other seasons and over multiple years will be required to investigate the temporal and interannual variability in ocean heat transport to the DIT. The extent to which warm ocean waters that enter the sub-glacial trough can reach the grounding line is also unknown and requires further investigation. More observations of water properties and bathymetry are needed across the continental shelf and beneath the Denman glacier. Some float profiles have linearly interpolated positions because they were collected under sea ice. However, the uncertainty in position has no impact on the net geostrophic volume and heat transport calculated here, as the position of the end-points of the transects are known. The transport estimates depend on the choice of reference level and on the treatment of the water column below the deepest common depth of each profile pair. Our estimates of the volume and heat transports, and their uncertainties, are based on conservative assumptions (Texts S3 and S4 in Supporting Information S1). The fact that the estimated transports are consistent with the exchange rate implied by satellite-derived basal melt rates provides additional confidence in our estimates.

These results add further evidence to show that East Antarctic ice shelves, once believed to be isolated from warm ocean waters and therefore stable, are potentially vulnerable to ocean heat transport. Measurements at the Totten (Rintoul et al., 2016) and now Denman ice fronts confirm that warm water reaches the cavities beneath ice shelves formed by the two major drainages of the Aurora Basin, with its potential sea-level rise contribution of 5.1 m (Greenbaum et al., 2015). While the prograde bedrock slope extending 50 km inland of the Totten grounding line stabilizes that system (Morlighem et al., 2020), reducing the risk of imminent rapid retreat through the marine ice shelf instability mechanism (Weertman, 1974), the retrograde slope beneath Denman (Morlighem et al., 2020) makes it potentially unstable and at risk of rapid and irreversible retreat. Our results demonstrate that warm water reaches the cavity beneath the floating portion of the Denman Glacier, providing a possible trigger for ocean-driven retreat.

Data Availability Statement

The profiling float data used in this study are available from the Argo Global Data Repositories, (Argo, 2022): https://doi.org/10.17882/42182 and the seal data are available from the Marine Mammals Exploring the Oceans Pole to Pole data set: https://www.seanoe.org/data/00343/45461/.

Acknowledgments
We thank colleagues onboard *RV Shirase* for deploying the float on behalf of the Australian program, and the reviewers whose comments have improved this manuscript. This work was supported by the Antarctic Science Collaboration Initiative; the Australian Antarctic Program Partnership; CSIRO Oceans and Atmosphere; the Centre for Southern Hemisphere Oceans Research and the University of Tasmania (Graduate Research Scholarship).

References

Argo (2022). Argo float data and metadata from Global Data Assembly Centre (Argo GDAC). *SEANOE*. https://doi.org/10.17882/42182

Bernales, J., Rogozhina, I., & Thomas, M. (2017). Melting and freezing under Antarctic ice shelves from a combination of ice-sheet modelling and observations. *Journal of Glaciology*, *63*(240), 731–744. https://doi.org/10.1017/jog.2017.42

Brancato, V., Rignot, E., Milillo, P., Morlighem, M., Mouginot, J., An, L., et al. (2020). Grounding line retreat of Denman Glacier, East Antarctica, measured with COSMO-SkyMed radar interferometry data. *Geophysical Research Letters*, *47*(7), e2019GL086291. https://doi.org/10.1029/2019GL086291

Depoorter, M. A., Bamber, J. L., Griggs, J. A., Lenaerts, J. T. M., Ligtenberg, S. R. M., van den Broeke, M. R., & Moholdt, G. (2013). Calving fluxes and basal melt rates of Antarctic ice shelves. *Nature*, *502*(7469), 89–92. https://doi.org/10.1038/nature12567

Dutrieux, P., De Rydt, J., Jenkins, A., Holland, P. R., Kyung Ha, H., Lee, S. H., et al. (2014). Strong sensitivity of Pine Island Ice-Shelf melting to climatic variability. *Science*, *343*(6167), 174–178. https://doi.org/10.1126/science.1244341

Gade, H. (1979). Melting of ice in sea water: A primitive model with application to the Antarctic ice shelf and icebergs. *Journal of Physical Oceanography*, *9*(1), 189–198. https://doi.org/10.1175/1520-0485(1979)009<0189:moiisw>2.0.co;2

Greenbaum, J. S., Blankenship, D. D., Young, D. A., Richter, T. G., Roberts, J. L., Aitken, A. R. A., et al. (2015). Ocean access to a cavity beneath Totten Glacier in East Antarctica. *Nature Geoscience*, *8*(4), 294–298. https://doi.org/10.1038/ngeo2388

Herraiz-Borreguero, L., & Naveira Garabato, A. C. (2022). Poleward shift of Circumpolar Deep Water threatens the East Antarctic Ice Sheet. *Nature Climate Change*, *12*(8), 728–734. https://doi.org/10.1038/s41558-022-01424-3

Jacobs, S. S., Jenkins, A., Giulivi, C. F., & Dutrieux, P. (2011). Stronger ocean circulation and increased melting under Pine Island Glacier ice shelf. *Nature Geoscience*, *4*(8), 519–523. https://doi.org/10.1038/ngeo1188

Jenkins, A. (1999). The impact of melting ice on ocean waters. *Journal of Physical Oceanography*, *29*(9), 2370–2381. https://doi.org/10.1175/15200485(1999)029<2370:TIOMIO>2.0.CO;2

Jenkins, A. (2011). Convection-driven melting near the grounding lines of Ice Shelves and Tidewater Glaciers. *Journal of Physical Oceanography*, *41*(12), 2279–2294. https://doi.org/10.1175/JPO-D-11-03.1

Jenkins, A., & Jacobs, S. (2008). Circulation and melting beneath George VI Ice Shelf, Antarctica. *Journal of Geophysical Research*, *113*(C4), C04013. https://doi.org/10.1029/2007JC004449

Klatt, O., Boebel, O., & Fahrbach, E. (2007). A profiling float's sense of ice. *Journal of Atmospheric and Oceanic Technology*, *24*(7), 1301–1308. https://doi.org/10.1175/JTECH2026.1

Liang, Q., Zhou, C., & Zheng, L. (2021). Mapping Basal Melt Under the Shackleton Ice Shelf, East Antarctica, from CryoSat-2 Radar Altimetry. *IEEE Journal of Selected Topics in Applied Earth Observations and Remote Sensing*, *14*, 5091–5099. https://doi.org/10.1109/jstars.2021.3077359

MacAyeal, D. R. (1984). Thermohaline circulation below the Ross Ice Shelf: A consequence of tidally induced vertical mixing and basal melting. *Journal of Geophysical Research*, *89*(C1), 597. https://doi.org/10.1029/JC089iC01p00597

Makinson, K. (2002). Modeling tidal current profiles and vertical mixing beneath Filchner-Ronne Ice Shelf, Antarctica. *Journal of Physical Oceanography*, *32*(1), 202–215. https://doi.org/10.1175/1520-0485(2002)032<0202:mtcpav>2.0.co;2

Miles, B. W. J., Jordan, J. R., Stokes, C. R., Jamieson, S. S. R., Gudmundsson, G. H., & Jenkins, A. (2021). Recent acceleration of Denman Glacier (1972–2017), East Antarctica, driven by grounding line retreat and changes in ice tongue configuration. *The Cryosphere*, *15*(2), 663–676. https://doi.org/10.5194/tc-15-663-2021

Morlighem, M. (2020). *MEaSUREs BedMachine Antarctica, version 2*. NASA National Snow and Ice Data Center Distributed Active Archive Center. https://doi.org/10.5067/E1QL9HFQ7A8M

Morlighem, M., Rignot, E., Binder, T., Blankenship, D. D., Drews, R., Eagles, G., et al. (2020). Deep glacial troughs and stabilizing ridges unveiled beneath the margins of the Antarctic ice sheet. *Nature Geoscience*, *13*(2), 132–137. https://doi.org/10.1038/s41561-019-0510-8

Nakayama, Y., Cai, C., & Seroussi, H. (2021). Impact of subglacial freshwater discharge on Pine Island ice shelf. *Geophysical Research Letters*, *48*(18), e2021GL093923. https://doi.org/10.1029/2021GL093923

Rignot, E., & Jacobs, S. S. (2002). Rapid bottom melting widespread near Antarctic Ice sheet grounding lines. *Science*, *296*(5575), 2020–2023. https://doi.org/10.1126/science.1070942

Rignot, E., Jacobs, S., Mouginot, J., & Scheuchl, B. (2013). Ice shelf melting around Antarctica. *Science*, *341*(6143), 266–270. https://doi.org/10.1126/science.1235798

Rignot, E., Mouginet, J., Scheuchl, B., van den Broeke, M., van Wessem, M. J., & Morlighem, M. (2019). Four decades of Antarctic Ice Sheet mass balance from 1979–2017. *Proceedings of the National Academy of Sciences of the United States of America*, *116*(4), 1095–1103. https://doi.org/10.1073/pnas.1812883116

Rintoul, S. R., Silvano, A., Pena-Molino, B., van Wijk, E., Rosenberg, M., Greenbaum, J. S., & Blankenship, D. D. (2016). Ocean heat drives rapid basal melt of Totten Ice Shelf. *Science Advances*, *2*(12), e1601610. https://doi.org/10.1126/sciadv.1601610

Silvano, A., Rintoul, S. R., Pena-Molino, B., & Williams, G. D. (2017). Distribution of water masses and meltwater on the continental shelf near the Totten and Moscow University ice shelves. *Journal of Geophysical Research: Oceans*, *122*(3), 2050–2068. https://doi.org/10.1002/2016JC012115

Thompson, S. S., Kulessa, B., Cornford, S., Luckman, A., & Halpin, J. (2021). *Glaciological setting of the Queen Mary and Knox coasts, East Antarctica, over the past 60 years, and implied dynamic stability of the Shackleton system*. The Cryosphere Discuss. https://doi.org/10.5194/tc-2021-265

Wallace, L. O., van Wijk, E. M., Rintoul, S. R., & Hally, B. (2020). Bathymetry constrained navigation of Argo floats under sea ice on the Antarctic continental shelf. *Geophysical Research Letters*, *47*(11), e2020GL087019. https://doi.org/10.1029/2020GL087019

Weertman, J. (1974). Stability of the junction of an ice sheet and an ice shelf. *Journal of Glaciology*, *13*(67), 3–11. https://doi.org/10.1017/s0022143000023327

Wilson, N. J., & Straneo, F. (2015). Water exchange between the continental shelf and the cavity beneath Nioghalvfjerdsbræ (79 North Glacier). *Geophysical Research Letters*, *42*(18), 7648–7654. https://doi.org/10.1002/2015GL064944

Wong, A., Keeley, R., & Carval, T. (2021). *Argo data management team*. Argo Quality Control Manual for CTD and Trajectory Data. https://doi.org/10.13155/33951

Wåhlin, A. K., Steiger, N., Darelius, E., Assmann, K. M., Glessmer, M. S., Ha, H. K., et al. (2020). Ice front blocking of ocean heat transport to an Antarctic ice shelf. *Nature*, *578*(7796), 568–571. https://doi.org/10.1038/s41586-020-2014-5

Yamazaki, K., Aoki, S., Katshumata, K., Hirano, D., & Nakayama, Y. (2021). Multidecadal poleward shift of the southern boundary of the Antarctic Circumpolar Current off East Antarctica. *Science Advances*, *7*(24). https://doi.org/10.1126/sciadv.abf8755

Yamazaki, K., Aoki, S., Shimada, K., Kobayashi, T., & Kitade, Y. (2020). Structure of the subpolar gyre in the Australian Antarctic Basin derived from Argo floats. *Journal of Geophysical Research: Oceans*, *125*(8), e2019JC015406. https://doi.org/10.1029/2019JC015406

References From the Supporting Information

An, L., Rignot, E., Millan, R., Tinto, K. J., & Willis, J. (2019). Bathymetry of Northwest Greenland using "Ocean Melting Greenland" (OMG) high-resolution airborne gravity and other data. *Remote Sensing*, *11*(2), 131–147. https://doi.org/10.3390/rs11020131

Bailleul, F., Charrassin, J.-B., Monestiez, P., Roquet, F., Biuw, M., Guinet, C., et al. (2007). Successful foraging zones of southern elephant seals from the Kerguelen Islands in relation to oceanographic conditions. *Philosophical Transactions of the Royal Society B: Biological Sciences*, *362*(1487), 2169–2181. https://doi.org/10.1098/rstb.2007.2109

Jonsen, I. D., Patterson, T. A., Costa, D. P., Doherty, P. D., Godley, B. J., Grecian, W. J., et al. (2020). A continuous-time state-space model for rapid quality control of Argos locations from animal-borne tags. *Movement Ecology*, *8*(1), 31. https://doi.org/10.1186/s40462-020-00217-7

Roquet, F., Williams, G., Hindell, M., Harcourt, R., McMahon, C., Guinet, C., et al. (2014). A Southern Indian Ocean database of hydrographic profiles obtained with instrumented elephant seals. *Scientific Data*, *1*, 140028. https://doi.org/10.1038/sdata.2014.28

Siegelman, L., Roquet, F., Mensah, V., Rivière, P., Pauthenet, E., Picard, B., & Guinet, C. (2019). Correction and accuracy of high- and low-resolution CTD data from animal-borne instruments. *Journal of Atmospheric and Oceanic Technology*, *36*(5), 745–760. https://doi.org/10.1175/JTECH-D-18-0170.1